Solution Structure of the Sulfite Reductase Flavodoxin-like Domain from *Escherichia coli*[†,‡]

Nathalie Sibille,[§,||] Martin Blackledge,[§] Bernhard Brutscher,[§] Jacques Covès,[⊥] and Beate Bersch*[,§]

Laboratoire de Résonance Magnétique Nucléaire and Laboratoire des Protéines Membranaires, Institut de Biologie Structurale-Jean-Pierre Ebel, 41 rue Jules Horowitz, UMR 5075 CEA-CNRS-UJF, 38027 Grenoble Cedex 1, France

Received March 8, 2005; Revised Manuscript Received May 9, 2005

ABSTRACT: The flavoprotein moiety of *Escherichia coli* sulfite reductase (SiR-FP) is homologous to electron transfer proteins such as cytochrome-P450 reductase (CPR) or nitric oxide synthase (NOS). We report on the three-dimensional structure of SiR-FP18, the flavodoxin-like domain of SiR-FP, which has been determined by NMR. In the holoenzyme, this domain plays an important role by shuttling electrons from the FAD to the hemoprotein (the β-subunit). The structure presented here was determined using distance and torsion angle information in combination with residual dipolar couplings determined in two different alignment media. Several protein−FMN NOEs allowed us to place the prosthetic group in its binding pocket. The structure is well-resolved, and ^{15}N relaxation data indicate that SiR-FP18 is a compact domain. The binding interface with cytochrome *c*, a nonphysiological electron acceptor, has been determined using chemical shift mapping. Comparison of the SiR-FP18 structure with the corresponding domains from CPR and NOS shows that the fold of the protein core is highly conserved, but the analysis of the electrostatic surfaces reveals significant differences between the three domains. These observations are placed in the physiological context so they can contribute to the understanding of the electron transfer mechanism in the SiR holoenzyme.

In *Escherichia coli*, sulfur assimilation implies the six-electron reduction of sulfite to sulfide (*1*). This reaction is catalyzed by the enzyme sulfite reductase (SiR),[1] a multimeric hemoflavoprotein with probably an $\alpha_8\beta_8$ quaternary structure rather than the commonly accepted $\alpha_8\beta_4$ (*2*, *3*). The flavoprotein component (SiR-FP) of the enzyme contains two prosthetic groups: one FAD (flavin adenine dinucleotide) and one FMN (flavin mononucleotide) (*4*, *5*). SiR-FP belongs to a family of electron transfer flavoproteins that includes human NADPH-cytochrome P450 reductase (CPR), nitric oxide synthase (NOS), and *Bacillus megaterium* cytochrome P450 (P450-BM3) (*6*−*8*), as well as two other proteins identified in humans, a putative methionine synthase reductase (MSR) (*9*, *10*) and a cytoplasmic protein NR1, with yet unknown function, that is expressed in cancer cells (*11*). All these proteins bind the same prosthetic groups and possess an NADPH binding site. The two flavins are bound by different structural domains: FAD is associated with a ferredoxin-NADP$^+$ reductase (FNR)-like domain which also contains the NADPH binding site, whereas the FMN-binding domain is homologous to bacterial flavodoxins. These protein fragments are linked by the connecting domain. The physiological role of these flavoproteins consists of the transfer of electrons from the NADPH via the FAD and the FMN to a heme-containing acceptor protein, which catalyzes the final reduction reaction. In the case of SiR, the hemoprotein component (SiR-HP) or β-subunit contains one [Fe_4S_4] cluster coupled to a siroheme (*12*). The structural and catalytic properties of SiR-HP have been studied in detail (*12*−*14*).

One unique feature of the flavoprotein component of SiR is its oligomeric quaternary structure. Using limited proteolysis, Covès et al. (*15*) identified the 52 N-terminal residues of SiR-FP that are responsible for the octamerization and, consequently, succeeded in obtaining a monomeric but highly active analogue named SiR-FP60, according to its apparent molecular weight (*16*). More recently, the crystal structure of SiR-FP60 has been determined (*17*). As expected, the FNR-like FAD-binding domain and, to a lesser extent, the connecting domain showed significant structural resemblance to the corresponding domains in CPR (*18*) and NOS (*19*, *20*). However, no electron density could be detected for the flavodoxin-like domain, certainly because of its high mobility with respect to the rest of the molecule (*17*). To complete the structure of SiR-FP, an NMR study of an 18 kDa monomeric version of the flavodoxin-like domain of SiR-FP, named SiR-FP18, was initiated.

[†] This work was supported by the Centre National de la Recherche Scientifique (CNRS) and the Commissariat à l'Energie Atomique (CEA).

[‡] The molecular coordinates and the NMR constraints have been deposited with the Protein Data Bank as entry 1YKG.

* To whom correspondence should be addressed. Telephone: (33) 4 39 78 48 25. Fax: (33) 4 38 78 54 94. E-mail: beate.bersch@ibs.fr.

[§] Laboratoire de Résonance Magnétique Nucléaire.

[||] Present address: Bijvoet Center for Biomolecular Research, Utrecht University, Padualaan 8, 3584 CH Utrecht, The Netherlands.

[⊥] Laboratoire des Protéines Membranaires.

[1] Abbreviations: CPR, cytochrome P450 reductase; CSI, chemical shift index; FAD, flavin adenine dinucleotide; FMN, flavin mononucleotide; NOE, nuclear Overhauser effect; NOS, nitric oxide synthase; P450-BM3, *Bacillus megaterium* cytochrome P450; RDC, residual dipolar coupling; SiR, sulfite reductase holoenzyme; SiR-FP, sulfite reductase flavoprotein component; SiR-FP18, sulfite reductase FMN domain; SiR-HP, sulfite reductase hemoprotein component.

10.1021/bi050437p CCC: $30.25
Published on Web 06/04/2005

In our previous work (*21*), we determined the global fold of SiR-FP18 by comparing experimental NMR data with a homology model calculated using the crystallographic structures of the flavodoxin-like domains from CPR and P450-BM3 (*22*, *23*). We now report on the high-resolution structure of SiR-FP18, determined by NMR as well as on the backbone dynamics of the protein as deduced from ^{15}N relaxation. In addition, we studied the interaction of SiR-FP18 with bovine heart cytochrome *c*, an artificial electron acceptor. These data are interpreted and discussed in the context of the whole electron transfer complex, in which the flavodoxin-like domain plays a fundamental role by shuttling the electrons from the FNR-like domain to the hemoprotein moiety.

MATERIALS AND METHODS

Sample Preparation. Isotopically ^{15}N-labeled, doubly ^{15}N- and ^{13}C-labeled, and triply ^{2}H-, ^{15}N-, and ^{13}C-labeled samples of oxidized SiR-FP18, spanning amino acids 52−218 of the SiR flavoprotein moiety, were obtained as described elsewhere (*21*).

All NMR samples used for NOE collection were prepared at a concentration around 1.8 mM in 100 mM potassium phosphate buffer (pH 7.0) with 0.02% NaN_2 in either a 90% H_2O/10% D_2O mixture or 100% D_2O. Samples were stored under argon in a sealed NMR tube. For the interaction studies, a 1 mM sample of oxidized, ^{15}N-labeled SiR-FP18 in 20 mM phosphate buffer (pH 7.0) was titrated with a 10 mM bovine heart cytochrome *c* solution (obtained from Sigma). The variation of both the ^{1}H and ^{15}N chemical shifts was calculated from the Euclidian distance formula:

$$\Delta_{ave} = \sqrt{(\Delta\delta_H)^2 + \left(\frac{\gamma_N}{\gamma_H}\Delta\delta_N\right)^2}$$

NMR Spectroscopy. The complete resonance assignment of SiR-FP18, as well as the measurement of trans-H-bond scalar couplings (*24*), has been reported previously (*21*, *25*). Two sets of backbone RDCs have been measured in filamentous bacteriophage Pf1 liquid crystal (*26*) and in a mixture of 5% $C_{12}E_5$ and hexanol with $r = 0.96$ (*27*). Sample conditions and experimental details are given in detail elsewhere (*21*, *28*).

All NMR experiments described here were carried out at 303 K, on Varian Inova spectrometers operating at a proton frequency of 800 or 600 MHz and equipped with triple-resonance (^{1}H, ^{13}C, and ^{15}N) probes, including shielded *z*-gradients. All data were processed with Felix (Accelrys Inc.). Typically, a 90°-shifted squared sine-bell apodization function was applied to the time domain data prior to Fourier transformation. Residual water suppression was achieved using a sine-bell convolution.

Heteronuclear ^{15}N-edited three-dimensional (3D) NOESY-HSQC and ^{13}C-edited 3D NOESY-HSQC experiments were carried out at 800 MHz on a ^{15}N- and ^{13}C-labeled sample. In addition, a homonuclear two-dimensional (2D) NOESY experiment was carried out in D_2O and at 800 MHz for the detection of NOEs involving aromatic protons. The NOE mixing time for these three experiments was set to 100 ms. For each experiment, a first-order polynomial baseline correction was applied in the direct dimension, and a second-order polynomial baseline correction was applied in the indirect ^{1}H dimension.

The heteronuclear $^{1}H-^{15}N$ NOE was determined from two experiments with on- and off-resonance ^{1}H saturation which were recorded in an interleaved manner. The saturation time was set to 3.5 s and the recycle delay to 7 s.

NOE Distance Measurements. NOE distance restraints were obtained by manually assigning the cross-peaks from the three NOE experiments. Calibration was adjusted on $H_N^i-H_N^{i+1}$ peak volumes in α-helices for which the average distance was estimated to be 2.8 Å (*29*). Distances involving more than one proton were estimated using pseudoatom and multiplicity ($Z = n_I n_S$) corrections (*29*).

For the ^{13}C 3D NOESY-HSQC and the two-dimensional NOESY experiments, distances between methyl groups in valine or leucine residues or between aromatic protons were used for NOE calibration.

Structure Calculations. Structure calculations were performed using a two-step restrained molecular dynamics procedure. In a first step, a structural ensemble is calculated from randomized initial Cartesian coordinates using Discover 2.98 (Accelrys Inc.) and a classical simulating annealing calculation (*30*). Structural restraints comprise NOE-derived distances (ambiguous and unambiguous), backbone torsion angles obtained from chemical shift values using TALOS (*31*), and hydrogen bond restraints from the measurement of trans-H-bond scalar couplings (*21*). The 20 best structures as defined from the total experimental target function were selected for refinement against RDC restraints.

In the second step, the selected structures are refined using all the restraints mentioned above, combined with RDC restraints, using SCULPTOR (*32*); 130 $^{1}D_{NH}$, 127 $^{1}D_{COCA}$, and 131 $^{1}D_{COHN}$ RDC restraints could be measured in a filamentous bacteriophage Pf1 liquid crystal and 137 $^{1}D_{NH}$, 136 $^{1}D_{COCA}$, and 136 $^{1}D_{COHN}$ RDC restraints in a 5% $C_{12}E_5$/hexanol mixture with $r = 0.96$. The SCULPTOR calculation consists of three steps. The molecular coordinates are initially fixed, while the alignment tensor parameters evolve under the influence of RDCs measured from sites present in secondary structure elements. This step is composed of a sampling period of 4 ps at 300 K, followed by 3 ps at 200 K and conjugate gradient minimization. For each structure, the most appropriate starting point for the tensor optimization is thus defined. The molecule is then released, and the tensor and the molecule evolve under the influence of the same RDC restraints and the complete restraint set from step 1 during 9.3 ps at a temperature of 1000 K. During this period, k_{RDC} is increased from the initial value of 0.1 kcal mol^{-1} Hz^{-2} to the final value of 1.0 kcal mol^{-1} Hz^{-2}. This is followed by a 2.7 ps cooling period to 100 K and energy minimization. This step refines both the local structure and the tensor simultaneously (*33*). At this point, the remaining RDC restraints are introduced and both the tensor and conformation evolve freely during 24 ps at 1000 K, during which time k_{NOE}, k_{H-bond}, k_{dihe}, and k_{RDC} were again increased from their initial values (0.25 kcal mol^{-1} Å^{-2}, 0.25 kcal mol^{-1} Å^{-2}, 1.0 kcal mol^{-1} deg^{-2}, and 0.1 kcal mol^{-1} Hz^{-2}, respectively) to their final values (25 kcal mol^{-1} Å^{-2}, 25 kcal mol^{-1} Å^{-2}, 100 kcal mol^{-1} deg^{-2}, and 1.0 kcal mol^{-1} Hz^{-2}, respectively). Following the sampling period, the system was cooled to 100 K over 2.7 ps and the system again minimized using a conjugate gradient algorithm. This

calculation was repeated three times for each initial structure using different initial atomic velocity distributions. Fifteen structures were selected on the basis of the lowest total target function comprising NOE, backbone torsion, hydrogen bonding, and RDC restraints but originating from different initial structures. These structures were then refined in a complete force field including Coulombic and Lennard-Jones interactions, using a distance-dependent dielectric constant and reduced charges on solvent-exposed polar side chains (*34*). Structures evolved for 3.75 ps at 750 K under the influence of all NMR-derived restraints with the force constants k_{NOE}, k_{H-bond}, k_{dihe}, and k_{RDC} set to 12.5 kcal mol^{-1} Å^{-2}, 12.5 kcal mol^{-1} Å^{-2}, 50 kcal mol^{-1} deg^{-2}, and 0.5 kcal mol^{-1} Hz^{-2}, respectively. The final structural ensemble was obtained after cooling to 100 K followed by energy minimization. The molecular coordinates of the 15 selected structures have been deposited in the Protein Data Bank (PDB) as entry 1YKG.

Structure Visualization and Comparison. Structures were visualized using either InsightII (Accelrys Inc.) or DeepView (*35*). The latter was also used to compare the structure of SiR-FP18 with the structural homologues (rat CPR, PDB entry 1AMO; the FMN-binding domain of human CPR, PDB entry 1B1C; rat neuronal NOS, PDB entry 1TLL; and the complex of the heme and FMN domains of P450-BM3, PDB entry 1BVY) and to analyze its interaction with SiR-FP60 (PDB entry 1DDG).

RESULTS

Solution Structure Determination. We have determined the structure of SiR-FP18 in solution using liquid-state NMR spectroscopy. The assignment of ^{1}H, ^{13}C, and ^{15}N chemical shifts was reported previously and was published in the BMRB database as entry 4985 (*25*). This was now completed by the determination of the aromatic ring protons and of some proton frequencies of the FMN, enabling the placement of this prosthetic group within the protein using intermolecular NOEs.

The structure was calculated using a two-step procedure employing first Discover 2.98 (Accelrys Inc.) and then SCULPTOR (*32*) for structure refinement. In the first structure calculation step, the global fold of SiR-FP18 was determined de novo using 1114 useful, manually assigned distance restraints from the ^{15}N 3D NOESY-HSQC and ^{13}C 3D NOESY-HSQC and 2D NOESY experiments, 216 backbone torsion angle restraints determined from TALOS (*31*), and 119 hydrogen bond distance restraints based on measured $^{3h}J_{NC}$ couplings (*21*). The distribution of the 871 (nonredundant) unambiguous distance restraints is shown in Figure S1 of the Supporting Information. In the second step, 20 structures selected according to the experimental energy were further refined by the additional use of 786 residual dipolar coupling (RDC) restraints ($^{1}D_{HN}$, $^{2}D_{C'HN}$, and $^{1}D_{C'C\alpha}$) measured in two different alignment media, combined with the restraints used in the previous Discover calculation. As expected, introduction of RDC restraints resulted in a much better resolution of the backbone (rmsd of 0.55 Å compared to a rmsd of 1.03 Å) without significant violations of the independently identified distance and angular restraints. The resulting ensemble of 15 low-energy structures was further refined using a distance-dependent dielectric constant and reduced charges on solvent-exposed polar side chains. The axial and rhombic components of the two different molecular alignment tensors, which evolved simultaneously with the molecular coordinates, converged to an A_a of -18.9 ± 0.25 and an A_r of -11.6 ± 0.16 for the phage sample and an A_a of -19.2 ± 0.09 and an A_r of -10.8 ± 0.11 for the alcohol sample. Structural statistics of the final calculation are shown in Table 1.

Table 1: Statistics for the Final Structural Ensemble

coordinate precision (residues 63−208)	
rmsd for C′, Cα, N (Å)	0.55 ± 0.14
rmsd for heavy atoms (Å)	1.18 ± 0.18
structural statistics	
energy (kcal/mol)	
bond	36 ± 3
angle	261 ± 23
dihedral	196 ± 11
out-of-plane	13 ± 3
H-bond	−4 ± 12
VDW	−347 ± 26
electrostatic	−1868 ± 22
violation energy (kcal/mol[a])	460 ± 41
total	−1254 ± 92
experimental statistics	
no. of distance violations > 0.2 Å	26 ± 5
alignment tensor	
A_a (phage sample)	−18.9 ± 0.25
A_r (phage sample)	−11.6 ± 0.16
A_a (alcohol sample)	−19.2 ± 0.09
A_r (alcohol sample)	−10.8 ± 0.11
Ramachandran analysis (PROCHECK)	
residues in most favored regions (%)	91.1
residues in additional allowed regions (%)	7.6
residues in generously allowed regions (%)	0.8
residues in disallowed regions (%)	0.6

[a] Force constants used: $k_{NOE} = 12.5$ kcal mol^{-1} Å^{-2}, $k_{dihe} = 50$ kcal mol^{-1} rad^{-2}, and $k_{RDC} = 0.5$ kcal mol^{-1} Hz^{-2}.

Description of the Overall Fold. The resulting structural ensemble comprises 15 structures, which are shown superposed in Figure 1A. The well-folded domain consists of residues 63−208, whereas residues 52−62 and 209−218, which were present in the molecular construct, are disordered. This was further confirmed by the ^{15}N relaxation data (see below). The overall structure of SiR-FP18 shows the characteristic fold of bacterial flavodoxins, which is also common to the FMN-binding domains of CPR (*18*, *22*), NOS (*20*), and P450-BM3 (*23*) (see Figure 1B). SiR-FP18 is composed of five α-helices numbered H1−H4 and H′ as well as six β-strands (numbered I−IV, Va, and Vb). Helix H′ and β-strand Va could not confidently be predicted from the initial analysis of chemical shifts and short-range NOEs presented previously (*21*). These two secondary structure elements are conserved in CPR and NOS but not in P450-BM3. The high-resolution structure presented here allows us to identify the short helix H′ which corresponds to residues K103−A106, situated between strands II and III at the bottom of the SiR-FP18 structure, opposite from the FMN binding site. β-Strand Va is oriented nearly perpendicular to the central β-sheet, but is hydrogen-bonded to strand IV by three hydrogen bonds.

Most of the loops connecting the secondary structure elements are well-defined, with rmsd values calculated for the backbone atoms (N, Cα, and C′) of individual residues below 0.7 Å. The only exception is the loop connecting helix H2 and β-strand IV where the rmsd exceeds 1.0 Å for

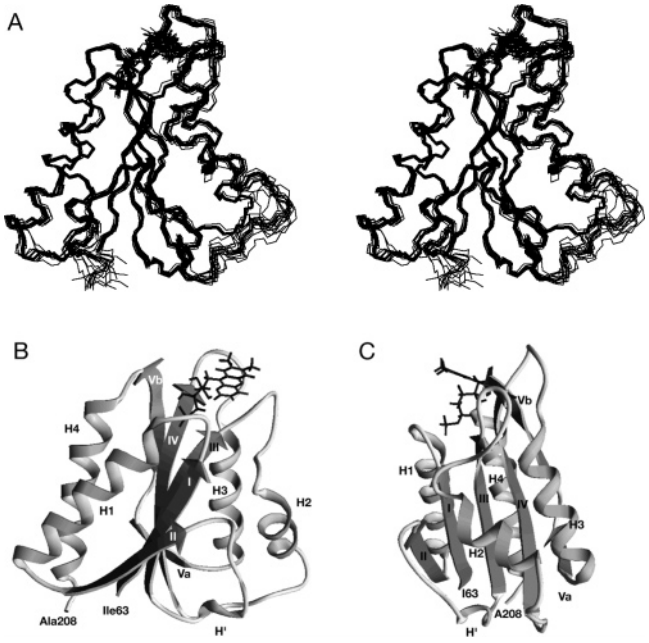

FIGURE 1: NMR structure of SiR-FP18. (A) Superposition of the final 15 structures on their mean. Shown are the backbone of residues 63−208 and the FMN cofactor. (B, C) Schematic representation of the SiR-FP18 fold and the localization of the FMN. Secondary structure elements are indicated as described in the text.

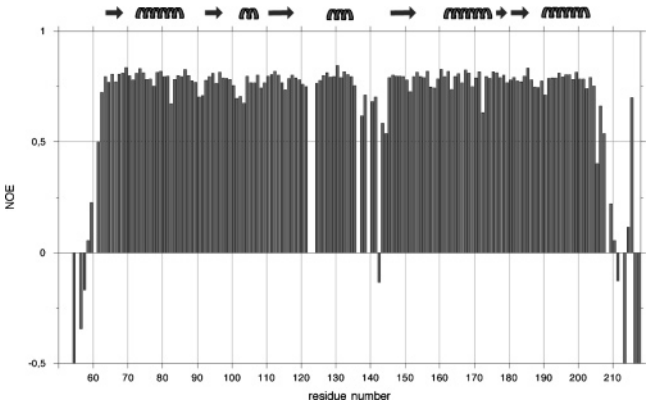

FIGURE 2: Backbone dynamics of SiR-FP18 sampled by heteronuclear $^{1}H-^{15}N$ NOE measured at 600 MHz. The NOE values are shown as a function of the protein sequence, and secondary structure elements are indicated. Note that N- and C-terminal residues have NOEs much lower than −0.5.

residues Ser136−Glu143. According to the relaxation measurements, this is due to significant backbone mobility (see below).

FMN Binding Site. We were able to assign all protons located on the isoalloxazine ring of the FMN cofactor as well as the two C_1 protons of the ribityl moiety. With this information in hand, we could identify 31 FMN−protein NOEs, which allowed us to place the isoalloxazine ring in the binding site. The isoalloxazine ring was found to interact with the loop following β-strand III, including Gly119 and the loop between β-strand IV and H3, containing the well-conserved Tyr157 (Tyr140 in CPR), which is in a stacking interaction with the aromatic ring system. The overall orientation of the isoalloxazine ring is quite well defined in the 15 final structures as shown in Figure 1A. The remaining protons of the ribityl moiety were not assigned as they were in severe overlap with proton resonances of the protein. To fix the ribityl and the phosphate group, we introduced three ambiguous distances between phosphate and Gln70, Asn73, and Ala74 amide protons. These amide groups were previously identified by their peculiar chemical shifts (>10 ppm), suggesting hydrogen bond formation with the phosphate group (*36*). In the crystal structures of CPR and NOS, the homologous residues are also involved in hydrogen bonds with the FMN phosphate group, further justifying the introduction of these constraints into our structure calculation.

NMR Relaxation Measurements. The mobility of the SiR-FP18 backbone has been studied using ^{15}N relaxation measurements. As can be seen from Figure 2, which shows the heteronuclear NOE values as a function of the protein sequence, the flavodoxin-like domain spanning residues 63−208 appears to be quite rigid. Analysis of the longitudinal and transversal relaxation rates using TENSOR (*37*) showed that the overall rotational tumbling of the molecule is best described by an axially anisotropic prolate model with the following rotational diffusion coefficients: $D_{||} = 20 \times 10^7$ s^{-1} and $D_{\perp} = 13.5 \times 10^7$ s^{-1} (indicating that SiR-FP18 is a monomeric protein in solution). Besides the N- and C-terminal residues, the overall value of the heteronuclear NOE exceeds 0.7 for most residues. The only exception is the loop between helix 2 and strand IV for which the NOE values are significantly lowered. In the case of Glu143, a negative NOE value has been measured, indicating significant backbone flexibility. It has to be noted that this loop bears the insertion of the autoinhibitory helix in NOS and that in the nNOS crystal structure it is not visible, certainly due to molecular motion (*20*).

Interaction Studies. SiR-FP18 is able to transfer electrons to cytochrome *c* in a nonphysiological reaction (*21*). This interaction was further characterized by NMR using chemical shift mapping. Upon titration of SiR-FP18 with 1, 2, and 4 molar equiv of bovin heart cytochrome *c*, very low variations of the average amide chemical shift of less than 0.05 ppm could be observed, indicating the transient nature of complex formation. This is shown as a function of the protein sequence in Figure S2 of the Supporting Information. Average amide chemical shift variations are mainly observed for residues Arg182, Asp184, and Ala185, and to a lesser extent for residues Ala148, Val149, and Lys165. Residues 165, 182, 184, and 185 are surface-exposed in SiR-FP18, and their location is highlighted in Figure 3. These residues are close to acidic cluster 1, situated between strand Vb and helix H4. This cluster has been identified in CPR as being responsible for the electron transfer to cytochrome P450 (*38*) (residues Asp207−Asp209 in CPR corresponding to Asp186−Glu188 in SiR-FP18). However, in CPR (*38*), nNOS (*39*), and bacterial flavodoxin (*40*), mutations in this cluster did not affect electron transfer with cytochrome *c*. As the interaction between SiR-FP18 and cytochrome *c* was found to be invisible at 100 mM phosphate buffer (results not shown), we propose that it is mainly driven by electrostatic interactions. Residues 182, 184, and 185 are situated in an area with predominantly negative charges which might facilitate the interaction with the positively charged cytochrome *c*. Residues 148 and 149, which have also been found to be influenced by the interaction with cytochrome *c*, are buried, but the amide groups of Val149 and Arg182 are only separated by ~5 Å.

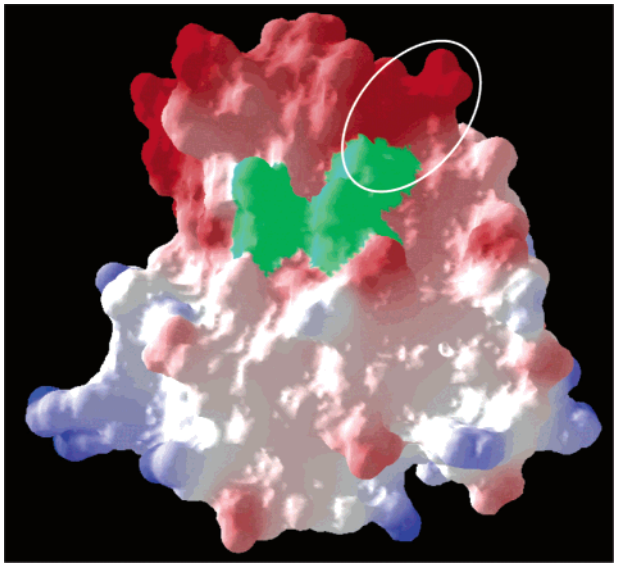

FIGURE 3: Chemical shift mapping of the interaction of SiR-FP18 with cytochrome *c*. SiR-FP18 is seen from the back with respect to the orientation shown in Figure 1. The exposed surface of residues which show a chemical shift variation due to the addition of cytochrome *c* is colored green. The localization of acidic cluster 1 is indicated. The surface of SiR-FP18 is colored with respect to the electrostatic potential ranging from −6 (red) to 6 kT (blue).

DISCUSSION

Knowledge of the molecular structure of SiR-FP18, the flavodoxin-like domain of the bacterial sulfite reductase, completes the structural information available so far on this huge multimeric enzyme. Previously, crystal structures have been determined for the β-subunit (SiR-HP; *12*−*14*) and a part of the flavoprotein, containing the FNR-like domain as well as the linker connecting the latter to the flavodoxin-like domain (*17*). In addition, structural information about homologous proteins has become available, allowing a much better understanding of the molecular processes involved in electron transfer. In this context, the flavodoxin-like domain plays a particularly important role, as it interacts with both the FNR domain of the flavoprotein moiety and the hemoprotein to shuttle electrons from the FAD to the heme. From results obtained independently by different groups, there is more and more experimental evidence that the interaction of the flavodoxin-like domain with both its partners involves the same surface region, suggesting a swinging motion of this domain within the electron transfer complex (*20*, *41*). Using the molecular structure we have determined, we address the process of this electron transfer in the case of SiR by comparing our results with those obtained on homologous molecules.

Comparison of SiR-FP18 with the Flavodoxin-like Domains from CPR and NOS. The backbone fold of the individual flavodoxin-like domains is remarkably similar. Superposing structurally homologous backbone atoms leads to molecular rmsd values of 1.38 Å for CPR (548 backbone atoms) and 1.12 Å for NOS (552 backbone atoms). A superposition of the three different flavodoxin-like domains is shown in Figure 4. SiR-FP18 seems to represent the core fold of the flavodoxin-like domains, whereas both CPR and NOS contain additional structural elements. In CPR, an N-terminal extension including an α-helix is involved in interdomain contacts with the connecting domain and a short insert between strands II and III forms an additional helical turn at the bottom of the molecule in the orientation of Figure 4. In NOS, an autoinhibitory insert is situated between helix H2 and β-strand IV. In SiR-FP18, the loop connecting strand Vb and helix 4 is shortened by two residues. This is an interesting observation as this loop is certainly involved in specific protein−protein interactions. In CPR, this loop contains acidic cluster 1 which has been suggested to interact with cytochrome P450 (*22*, *38*). In NOS, residues Leu920 and Cys921 situated in the same surface loop are involved in the interaction with the regulatory C-terminal tail which locks the FMN domain in the electron-accepting position (*20*) where the FMN can receive electrons from the FAD situated on the FNR-like domain.

The localization of the FMN with respect to the protein moiety is identical in the three proteins. Comparison of the amino acid sequences between different bacterial flavodoxins and flavodoxin-like domains reveals that two aromatic residues are very well conserved in the proximity of the FMN-binding site (residues Tyr140 and Tyr178 in CPR). However, in two proteins with known structure, the *Clostridium beijerinckii* flavodoxin (*42*) and SiR-FP, one of these conserved aromatic amino acids (Tyr140 of CPR) is replaced with an aliphatic residue: methionine in the case of *C. beijerinckii* flavodoxin and glutamine (Gln118) in SiR-FP. Figure 5A shows a detailed view of the FMN-binding pocket comparing the crystal structures of CPR (*22*) and NOS (*20*) with the NMR structure presented here. It can be seen that the backbone orientation and the position of most aromatic residues are nearly identical. The strictly conserved Tyr157 of SiR-FP18 is in a stacking interaction with the FMN ring as are the side chains of Tyr178 in CPR or Tyr889 in NOS. Phe181 of CPR, which has been reported to play an important role in FMN binding and catalytic activity by stabilizing the FMN-binding site (*43*), is superposable with Phe160 of SiR-FP18 or Phe892 of NOS. The surface-exposed His180 in CPR (His891 of NOS) is replaced with a phenylalanine in SiR-FP18. As already mentioned above, the highly conserved aromatic amino acid in the proximity of the FMN cofactor (Y140 of CPR or F809 of NOS) is replaced with Gln118 in SiR-FP. From Figure 5A, it becomes clear that one function of the conserved Tyr140 in CPR is the establishment of a hydrogen bond with the FMN phosphate group. Both in SiR-FP18 and in NOS, the same hydrogen bond with the FMN phosphate is formed with the side chain of a neighboring serine (S116 of SiR or S807 of NOS) found in the position of the OH group of Tyr140 of CPR. Remarkably, the same hydrogen bond with a serine is also found in *C. beijerinckii* flavodoxin.

In addition to the hydrogen bonds involving the FMN phosphate group, several other hydrogen bonds between the isoalloxazine ring and backbone atoms of the protein have been identified and are summarized in Figure 5B. These interactions are well conserved, and the same hydrogen bond pattern has been identified in human CPR (*22*) and in the flavodoxin from *Desulfovibrio vulgaris* (*44*). The only exception is the hydrogen bond to O4 on the isoalloxazine ring which does not occur in the SiR-FP18 structural ensemble. This might be due to the lack of experimental constraints for the backbone of G119, which, according to the CPR structure, should establish the hydrogen bond with O4.

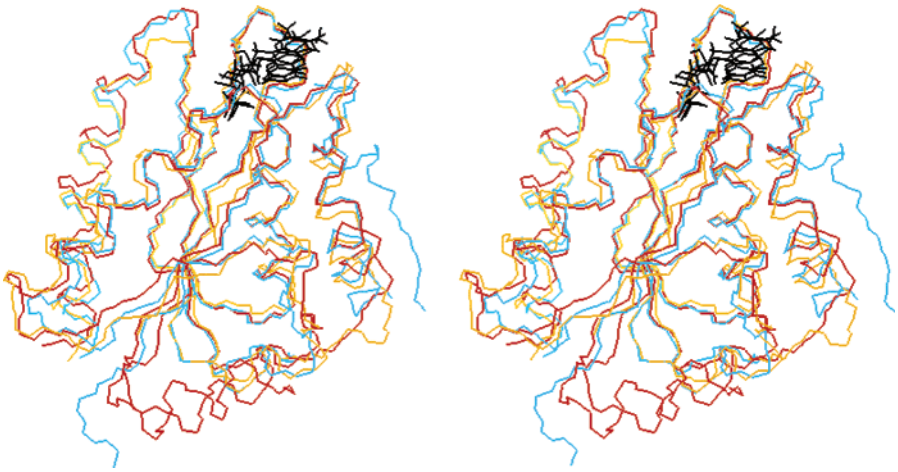

FIGURE 4: Structural comparison of FMN-binding domains. Stereoview of the superposition of the FMN-binding domains of human cytochrome P450 reductase (red), rat NO synthase (blue), and SiR-FP18 (orange). The cofactors of the three proteins are colored black.

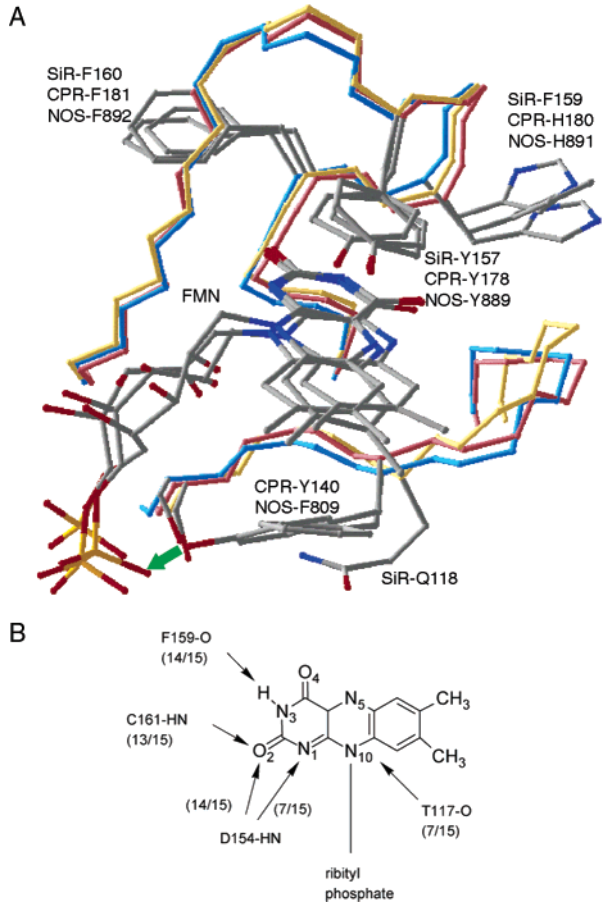

FIGURE 5: Detailed view of the FMN-binding site. (A) Structural comparison. The two loops surrounding the FMN-binding site are shown with the backbone in red (human CPR), blue (rat NOS), and yellow (SiR-FP18). They correspond to residues Ser116−Gly121 and Leu152−Gln162 (SiR-FP18 numbering). Side chains discussed in detail in the text and the FMN cofactors are colored in CPK mode, and the hydrogen bond to the FMN phosphate group is colored green. (B) Hydrogen bonds between the protein backbone and the isoalloxazine group found in the final structural ensemble. The frequency of occurrence throughout the ensemble is given in parentheses for each hydrogen bond.

It was mentioned above that Phe159 is surface-exposed in SiR-FP18. Inspection of the molecular surface seen from the right with respect to the orientation shown in Figure 1 reveals a second exposed phenylalanine (Phe135). These residues might play a role in hydrophobic protein−protein interactions. The two exposed side chains are localized in a convex surface region, which may exist to allow such interactions to occur. It might be worth considering that when SiR-FP18 is superposed with the flavodoxin-like domain of NOS (*20*), this surface forms the interface with the autoinhibitory helix, the presence of which has so far only been reported in NOS. In the case of SiR, there is no information available about the molecular organization of the holoenzyme, so we can only speculate about the role of this surface region.

Toward the Whole SiR Complex. With the resolution of the SiR-FP18 molecular structure, the major components interacting within the macromolecular complex of the *E. coli* sulfite reductase have now been structurally characterized. We will now consider putting together the information available from the individual fragments to gain insight into the fundamental process of electron transfer from NADPH to sulfite.

Much work has been devoted to the functional characterization of the individual fragments of SiR and their ability to transfer electrons to physiological or artificial electron acceptors. The SiR flavoprotein moiety is composed of the N-terminal octamerization domain, the FMN- and FAD-binding domains, and the connecting domain (*4*, *5*). The latter three domains are shared in CPR, NOS, and bacterial P450-BM3. A functional reconstitution of the flavoprotein moiety from SiR-FP23, the octameric FMN-binding domain, and SiR-FP43, the FAD-binding and connecting domain, could not be achieved (*15*). In the case of the bacterial flavocytochrome P450-BM3 and CPR, a functional complex, but with low activities, could be obtained from the separate domains (*45*, *46*). In the case of SiR, these protein fragments seem to be unable to interact with each other in solution. However, the individually produced octameric flavoprotein moiety (SiR-FP) was shown to be fully active by transferring electrons from the NADPH via the FAD and the FMN to SiR-HP, the physiological partner (*15*), to cytochrome P450c17 (*47*), or to cytochrome *c* (*15*). Further simplification of the flavoprotein moiety was achieved by the construction of a monomeric version, called SiR-FP60 (*16*). This protein lacks the N-terminal octamerization domain. Interestingly, SiR-FP60 could still reduce the physiological partner SiR-HP, but its activity was reduced by more than 80% when

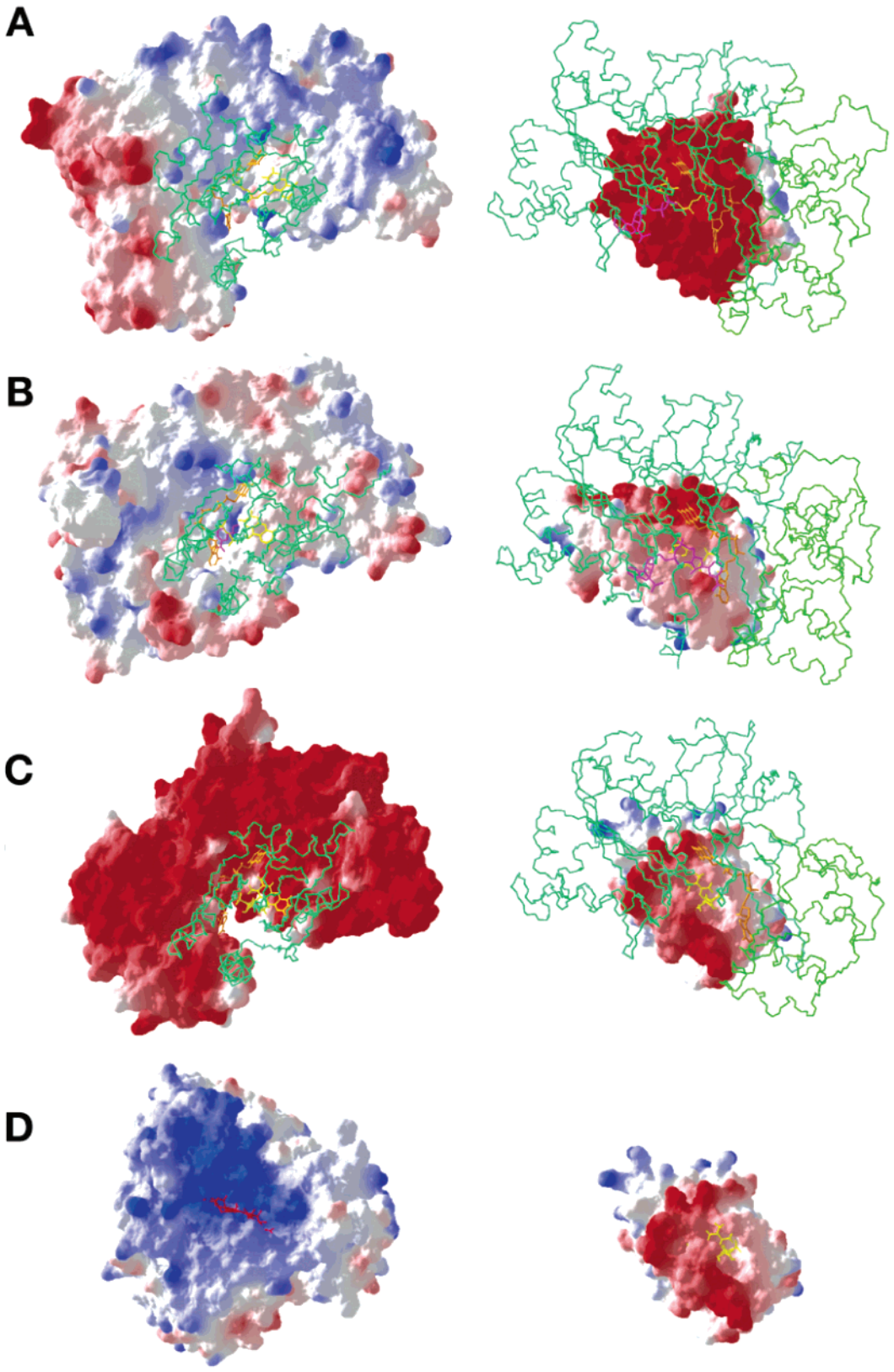

FIGURE 6: Interaction of the flavodoxin-like domain with its electron transfer partners. (A−C) Molecular interface between FMN- and FAD-binding domains. The molecular surfaces of the FAD-binding domain and the connecting domain are shown on the left and those of the FMN-binding domain on the right. The two views are related by a 180° rotation around a vertical axis. The backbone and the cofactor of the electron transfer partner are shown to indicate the relative localization of the two domains: (A) crystal structure of rat CPR (*18*), (B) crystal structure of rat nNOS (*20*), and (C) model of the SiR-FP interface constructed from superposition of the two independently determined molecular structures (ref *17* and this work) on the rat CPR coordinates. (D) Molecular surface of SiR-FP18 in the same orientation as in panel C on the right and SiR-HP with the prosthetic group exposed in the center on the left. Surfaces have been colored according to the electrostatic potential ranging from −6 (red) to 6 kT (blue); the cofactors are colored yellow (FMN), orange (FAD), pink (NADP), and red (siroheme). Backbone coordinates are colored green, with a slightly different color for the connecting domain.

compared to that of octameric SiR-FP (*3*). In addition, SiR-FP60 was no more able to reduce cytochrome P450c17 (*47*). In both cases, however, the physical interaction between flavo- and hemoprotein could be detected using immunoprecipitation (*47*). These observations indicate that either the presence of the octamerization domain or the octameric organization of the holoenzyme is essential for a productive electron transfer between flavo- and hemoprotein.

So far, there is no structural information available for the whole electron transfer complex of any homologous system. However, crystal structures have been determined for the flavoprotein part of rat CPR (*18*) and, more recently, of neuronal NOS (*20*). In addition, the structure of the flavodoxin-like domain of flavocytochrome P450-BM3 has been determined in complex with the fatty acid hydroxylase P450 (*23*). Thus, structural information is available for the flavodoxin-like domain in the electron accepting and electron donating position. It is remarkable that in both cases, the interface between the two protein domains involves the same surface region of the FMN domain. An analogous conclusion has been made by Hall et al. (*48*), who studied the interaction of *E. coli* flavodoxin with flavodoxin reductase and methionine synthase using NMR. They found that the two proteins bind to unique but overlapping sites on the flavodoxin close to the exposed edge of the FMN cofactor. Electron transfer seems to occur directly between the prosthetic groups, while the exposed edge of the FMN first interacts with the FAD from the FNR-like domain and then with the heme or the iron−sulfur cluster on the hemoprotein. This model precludes the formation of a stable ternary complex in which the flavodoxin-like domain simultaneously interacts with both its redox partners in an electron transfer compatible orientation. Therefore, a swinging motion of the flavodoxin-like domain has been suggested to enable the interaction with the two different redox partners (*20*, *41*).

Superposition of different structures of the flavoprotein moiety shows that the relative orientation of the FNR and the flavodoxin-like domains are conserved between CPR and NOS. However, some conformational diversity occurs which is in accordance with the rotation of the flavodoxin-like domain with respect to the FNR domain. Panels A and B of Figure 6 show the interface between the flavodoxin-like domain and both the FAD-binding and the connecting domain for CPR (*18*) and NOS (*20*). We also obtained the analogous interface in the case of SiR-FP, by superposition of the two molecular fragments on the CPR structure (Figure 6C). Comparison of the electrostatic surfaces of the protein domains reveals that there are striking differences between the three functionally homologous systems. Whereas in the case of CPR and NOS electrostatic interactions contribute to the stabilization of the electron transfer complex, this is completely excluded in the case of SiR, where both domains expose a highly negatively charged surface. This might be the reason that it has been impossible to reconstitute electron transfer between the isolated FNR and flavodoxin-like domains and why the flavodoxin-like domain of SiR-FP60 could not be detected in the crystal structure. In the whole complex, one role of the oligomerization domain could be to maintain the cohesion between the different flavin modules despite the unfavorable surface charges.

On the other hand, the interaction of SiR-FP18 with the electron-accepting hemoprotein (SiR-HP) was extremely strong, and the complex that was formed could be disrupted only by suspension in denaturing electrophoresis buffer (*21*). Figure 6D shows the supposed interaction surfaces between FMN and the heme domain. The two surfaces around the exposed prosthetic groups have highly complementary charges: the region around the FMN group is strongly acidic, whereas the surface around the iron−sulfur cluster and the siroheme exposes numerous positive charges. These strong electrostatic interactions may explain the stability of the observed complex.

With these observations in mind, it becomes very difficult to imagine how these different protein domains and subunits can come together to form a stable and functional multimeric complex and to predict the molecular events that can trigger the partial dissociation of the FMN domain from the interaction surface of the hemoprotein and make it swing back to the FNR-like domain. There is experimental evidence that in the holoenzyme, the interaction between the hemoprotein and the octameric flavoprotein moieties is weaker than between SiR-HP and SiR-FP18. For the crystallographic studies, SiR-HP has been purified from the holoenzyme in 4 M urea (*13*), whereas the complex with SiR-FP18 was completely resistant to even higher urea concentrations (*21*). In addition, the functional studies demonstrate the importance of the oligomeric nature of the SiR holoenzyme. One could speculate whether this oligomerization domain plays a specific role by tuning the interaction between the flavodoxin-like domain and SiR-HP. There must be a sophisticated interplay between the individual domains that regulates the sequential interaction of the FMN domain with its redox partners as a function of the redox state of the individual cofactors. Future structural studies may allow characterization of the subunit interactions within the oligomeric SiR complex to improve our understanding of the molecular basis of the electron transfer within this protein.

ACKNOWLEDGMENT

We are very grateful to E. Garcin and E. D. Getzoff for access to the NOS PDB coordinates before their release.

SUPPORTING INFORMATION AVAILABLE

Two figures showing the distribution of unambiguous NOEs as a function of the protein sequence and the chemical shift differences induced by the titration of SiR-FP18 with cytochrome *c*. This material is available free of charge via the Internet at http://pubs.acs.org.

REFERENCES

1. Kredich, N. M. (1996) in *Escherichia coli and Salmonella thyphimurium: Cellular and Molecular Biology* (Neidhardt, F. C., et al., Eds.) pp 514−527, ASM Press, Washington, DC.
2. Siegel, L. M., and Davis, P. S. (1974) Reduced nicotinamide adenine dinucleotide phosphate-sulfite reductase of enterobacteria. IV. The *Escherichia coli* hemoflavoprotein: Subunit structure and dissociation into hemoprotein and flavoprotein components, *J. Biol. Chem. 249*, 1587−1598.
3. Zeghouf, M., Fontecave, M., and Covès, J. (2000) A simplified functional version of the *Escherichia coli* sulfite reductase, *J. Biol. Chem. 275*, 37651−37656.
4. Eschenbrenner, M., Covès, J., and Fontecave, M. (1995) The flavin reductase activity of the flavoprotein component of sulfite reductase from *Escherichia coli*. A new model for the protein structure, *J. Biol. Chem. 270*, 20550−20555.

5. Eschenbrenner, M., Covès, J., and Fontecave, M. (1995) NADPH-sulfite reductase flavoprotein from *Escherichia coli*: Contribution to the flavin content and subunit interaction, *FEBS Lett. 374*, 82−84.
6. Karplus, P. A., and Bruns, C. M. (1994) Structure−function relations for ferredoxin reductase, *J. Bioenerg. Biomembr. 26*, 89−99.
7. Porter, T. D., and Kasper, C. B. (1986) NADPH-cytochrome P-450 oxidoreductase: Flavin mononucleotide and flavin adenine dinucleotide domains evolved from different flavoproteins, *Biochemistry 25*, 1682−1687.
8. Bredt, D. S., Hwang, P. M., Glatt, C. E., Lowenstein, C., Reed, R. R., and Snyder, S. H. (1991) Cloned and expressed nitric oxide synthase structurally resembles cytochrome P-450 reductase, *Nature 351*, 714−718.
9. Leclerc, D., Wilson, A., Dumas, R., Gafuik, C., Song, D., Watkins, D., Heng, H. H., Rommens, J. M., Scherer, S. W., Rosenblatt, D. S., and Gravel, R. A. (1998) Cloning and mapping of a cDNA for methionine synthase reductase, a flavoprotein defective in patients with homocystinuria, *Proc. Natl. Acad. Sci. U.S.A. 95*, 3059−3064.
10. Olteanu, H., and Banerjee, R. (2001) Human methionine synthase reductase, a soluble P-450 reductase-like dual flavoprotein, is sufficient for NADPH-dependent methionine synthase activation, *J. Biol. Chem. 276*, 35558−35563.
11. Paine, M. J., Garner, A. P., Powell, D., Sibbald, J., Sales, M., Pratt, N., Smith, T., Tew, D. G., and Wolf, C. R. (2000) Cloning and characterization of a novel human dual flavin reductase, *J. Biol. Chem. 275*, 1471−1478.
12. Crane, B. R., Siegel, L. M., and Getzoff, E. D. (1995) Sulfite reductase structure at 1.6 Å: Evolution and catalysis for reduction of inorganic anions, *Science 270*, 59−67.
13. Crane, B. R., Siegel, L. M., and Getzoff, E. D. (1997) Structures of the siroheme- and Fe_4S_4-containing active center of sulfite reductase in different states of oxidation: Heme activation via reduction-gated exogenous ligand exchange, *Biochemistry 36*, 12101−12119.
14. Crane, B. R., Siegel, L. M., and Getzoff, E. D. (1997) Probing the catalytic mechanism of sulfite reductase by X-ray crystallography: Structures of the *Escherichia coli* hemoprotein in complex with substrates, inhibitors, intermediates, and products, *Biochemistry 36*, 12120−12137.
15. Covès, J., Zeghouf, M., Macherel, D., Guigliarelli, B., Asso, M., and Fontecave, M. (1997) Flavin mononucleotide-binding domain of the flavoprotein component of the sulfite reductase from *Escherichia coli*, *Biochemistry 36*, 5921−5928.
16. Zeghouf, M., Fontecave, M., Macherel, D., and Covès, J. (1998) The flavoprotein component of the *Escherichia coli* sulfite reductase: Expression, purification, and spectral and catalytic properties of a monomeric form containing both the flavin adenine dinucleotide and the flavin mononucleotide cofactors, *Biochemistry 37*, 6114−6123.
17. Gruez, A., Pignol, D., Zeghouf, M., Covès, J., Fontecave, M., Ferrer, J. L., and Fontecilla-Camps, J. C. (2000) Four crystal structures of the 60 kDa flavoprotein monomer of the sulfite reductase indicate a disordered flavodoxin-like module, *J. Mol. Biol. 299*, 199−212.
18. Wang, M., Roberts, D. L., Paschke, R., Shea, T. M., Masters, B. S., and Kim, J. J. (1997) Three-dimensional structure of NADPH-cytochrome P450 reductase: Prototype for FMN- and FAD-containing enzymes, *Proc. Natl. Acad. Sci. U.S.A. 94*, 8411−8416.
19. Zhang, J., Martasek, P., Paschke, R., Shea, T., Masters, B. S. S., and Kim, J. J. (2001) Crystal structure of the FAD/NADPH-binding domain of rat neuronal nitric-oxide synthase. Comparisons with NADPH-cytochrome P450 oxidoreductase, *J. Biol. Chem. 276*, 37506−37513.
20. Garcin, E. D., Bruns, C. M., Lloyd, S. J., Hosfield, D. J., Tiso, M., Gachhui, R., Stuehr, D., Trainer, J. A., and Getzoff, E. D. (2004) Structural basis for isozyme-specific regulation of electron transfer in nitric-oxide synthase, *J. Biol. Chem. 279*, 37918−37927.
21. Champier, L., Sibille, N., Bersch, B., Brutscher, B., Blackledge, M., and Covès, J. (2002) Reactivity, secondary structure, and molecular topology of the *Escherichia coli* sulfite reductase flavodoxin-like domain, *Biochemistry 41*, 3770−3780.
22. Zhao, Q., Modi, S., Smith, G., Paine, M., McDonagh, P. D., Wolf, C. R., Tew, D., Lian, L. Y., Roberts, G. C., and Driessen, H. P. (1999) Crystal structure of the FMN-binding domain of human cytochrome P450 reductase at 1.93 Å resolution, *Protein Sci. 8*, 298−306.
23. Sevrioukova, I. F., Li, H., Zhang, H., Peterson, J. A., and Poulos, T. L. (1999) Structure of a cytochrome P450-redox partner electron-transfer complex, *Proc. Natl. Acad. Sci. U.S.A. 96*, 1863−1868.
24. Cordier, F., and Grzesiek, S. (1999) Direct observation of hydrogen bonds in proteins by interresidue $^{3h}J_{NC'}$ scalar couplings, *J. Am. Chem. Soc. 121*, 1601−1602.
25. Sibille, N., Covès, J., Marion, D., Brutscher, B., and Bersch, B. (2001) ^{1}H, ^{13}C and ^{15}N assignment of the flavodoxin-like domain of the *Escherichia coli* sulfite reductase, *J. Biomol. NMR 21*, 71−72.
26. Hansen, M. R., Mueller, L., and Pardi, A. (1998) Tunable alignment of macromolecules by filamentous phage yields dipolar coupling interactions, *Nat. Struct. Biol. 5*, 1065−1074.
27. Rückert, M., and Otting, G. (2000) Alignment of biological macromolecules in novel nonionic liquid crystalline media for NMR experiments, *J. Am. Chem. Soc. 122*, 7793−7797.
28. Sibille, N., Bersch, B., Covès, J., Blackledge, M., and Brutscher, B. (2002) Side chain orientation from methyl ^{1}H-^{1}H residual dipolar couplings measured in highly deuterated proteins, *J. Am. Chem. Soc. 124*, 14616−14625.
29. Neuhaus, D., and Williamson, M. P. (2000) *The Nuclear Overhauser Effect in Structural and Conformational Analysis*, 2nd ed., Wiley, New York.
30. Blackledge, M. J., Medvedeva, S., Poncin, M., Guerlesquin, F., Bruschi, M., and Marion, D. (1995) Structure and dynamics of ferrocytochrome c_{553} from *Desulfovibrio vulgaris* studied by NMR spectroscopy and restrained molecular dynamics, *J. Mol. Biol. 245*, 661−681.
31. Cornilescu, D., Delaglio, F., and Bax, A. (1999) Protein backbone angle restraints from searching a database for chemical shift and sequence homology, *J. Biomol. NMR 13*, 289−302.
32. Hus, J.-C., Marion, D., and Blackledge, M. (2000) De novo determination of protein structure by NMR using orientational and long-range order restraints, *J. Mol. Biol. 298*, 927−936.
33. Sibille, N., Pardi, A., Simorre, J. P., and Blackledge, M. (2001) Refinement of local and long-range structural order in theophylline-binding RNA using $^{13}C-^{1}H$ residual dipolar couplings and restrained molecular dynamics, *J. Am. Chem. Soc. 123*, 12135−12146.
34. Singh, U. C., and Kollman, P. A. (1983) An approach to computing electrostatic charges for macromolecules, *J. Comput. Chem. 5*, 129−145.
35. Guex, N., and Peitsch, M. C. (1997) SWISS-MODEL and the Swiss-PdbViewer: An environment for comparative protein modeling, *Electrophoresis 18*, 2714−2723.
36. Barsukov, I., Modi, S., Lian, L. Y., Sze, K. H., Paine, M. J., Wolf, C. R., and Roberts, G. C. (1997) ^{1}H, ^{15}N and ^{13}C NMR resonance assignment, secondary structure and global fold of the FMN-binding domain of human cytochrome P450 reductase, *J. Biomol. NMR 10*, 63−75.
37. Dosset, P., Hus, J. C., Blackledge, M., and Marion, D. (2000) Efficient analysis of macromolecular rotational diffusion from heteronuclear relaxation data, *J. Biomol. NMR 16*, 23−28.
38. Shen, A. L., and Kasper, C. B. (1995) Role of acidic residues in the interaction of NADPH-cytochrome P450 oxidoreductase with cytochrome P450 and cytochrome *c*, *J. Biol. Chem. 46*, 27475−27480.
39. Adak, S., Ghosh, S., Abu-Soud, H. M., and Stuehr, D. J. (1999) Role of reductase domain cluster 1 acidic residues in neuronal nitric-oxide synthase. Characterization of the FMN−FREE enzyme, *J. Biol. Chem. 274*, 22313−22320.
40. Jenkins, C. M., Genzor, C. G., Fillat, M. F., Waterman, M. R., and Gomez-Moreno, C. (1997) Negatively charged anabaena flavodoxin residues (Asp144 and Glu145) are important for reconstitution of cytochrome P450 17α-hydroxylase activity, *J. Biol. Chem. 272*, 22509−22513.
41. Munro, A. W., Leys, D. G., McLean, K. J., Marshall, K. R., Ost, T. W. B., Daff, S., Miles, C. S., Chapman, S. K., Lysek, D. A., Moser, C. C., Page, C. C., and Dutton, P. L. (2000) P450 BM3: The very model of a modern flavocytochrome, *Trends Biochem. Sci. 27*, 250−257.

42. Ludwig, M. L., Pattridge, P. A., Metzger, A. L., Dixon, M. M., Even, M., Feng, Y., and Swenson, R. P. (1997) Control of oxidation−reduction potentials in flavodoxin from *Clostridium beijerinckii*: The role of conformation changes, *Biochemistry 36*, 1259−1280.
43. Paine, M. J. I., Ayivor, S., Munro, A., Tsan, P., Lian, L.-Y., Roberts, G. C. K., and Wolf, C. R. (2001) Role of the conserved phenylalanine 181 of NADPH-cytochrome P450 oxidoreductase in FMN binding and catalytic activity, *Biochemistry 40*, 13439−13447.
44. Watt, W., Tulinsky, A., Swenson, R. P., and Watenpaugh, K. D. (1991) Comparison of the crystal structures of a flavodoxin in its three oxidation states at cryogenic temperatures, *J. Mol. Biol. 218*, 195−208.
45. Sevrioukova, I., Truan, G., and Peterson, J. A. (1997) Reconstitution of the fatty acid hydroxylase activity of cytochrome P450 BM-3 utilizing its functional domains, *Arch. Biochem. Biophys. 340*, 231−238.
46. Smith, G. C., Tew, D. G., and Wolf, C. R. (1994) Dissection of NADPH-cytochrome P450 oxidoreductase into distinct functional domains, *Proc. Natl. Acad. Sci. U.S.A. 91*, 8710−8714.
47. Zeghouf, M., Defaye, G., Fontecave, M., and Covès, J. (1998) The flavoprotein component of the *Escherichia coli* sulfite reductase can act as a cytochrome P450c17 reductase, *Biochem. Biophys. Res. Commun. 246*, 602−605.
48. Hall, D. A., Vander Kooi, C. W., Stasik, C. N., Stevens, S. Y., Zuiderweg, E. R. P., and Matthews, R. G. (2001) Mapping the interactions between flavodoxin and its physiological partners flavodoxin reductase and cobalamin-dependent methionine synthase, *Proc. Natl. Acad. Sci. U.S.A. 98*, 9521−9526.

BI050437P